THE ASTROPHYSICAL JOURNAL, 411:247–259, 1993 July 1

HIGH-RESOLUTION H I OBSERVATIONS OF H II REGIONS. III. PHOTODISSOCIATION REGIONS AND THE MAGNETIC FIELD NEAR ORION B

PAUL P. VAN DER WERF
Max-Planck-Institut für extraterrestrische Physik, Giessenbachstraße, D-8046 Garching bei München, Germany
W. M. GOSS
National Radio Astronomy Observatory, P.O. Box 0, Socorro, NM 87801
CARL HEILES
University of California, Astronomy Department, Berkeley, CA 94720
R. M. CRUTCHER
University of Illinois, 103 Astronomy Building, 1002 West Green Street, Urbana, IL 61801
AND
T. H. TROLAND
University of Kentucky, Department of Physics and Astronomy, Lexington, KY 40506
Received 1992 May 20; accepted 1993 January 5

ABSTRACT

H I observations of the H II region Orion B are presented with an angular resolution of 50″ (0.1 pc) and velocity resolution of 0.64 km s^{-1}. Three kinematically distinct H I layers are detected in absorption. It is argued that one of these H I components originates in a photodissociation region (PDR) directly outside the ionization front in front of the H II region. In addition to the H I absorption, H I emission is detected, most likely originating in a PDR behind the H II region. Combining the H I emission and absorption data yields the conclusion that a range of temperatures exists in the PDRs, a conclusion corroborated by existing [C II] 158 μm line measurements of the PDRs. While the H I *absorption* data show the presence of gas colder than $\sim$20 K (which is too cold to contribute significantly to the [C II] emission), the H I and [C II] data can be brought in agreement if the *emitting* H I is a temperature of at least several hundred degrees. These results are interpreted in terms of a clumpy PDR model, where the colder gas is located in dense clumps, which are embedded in a warmer, low-density interclump medium.

An analysis of the Zeeman effect as determined from the observed circular polarization yields line-of-sight magnetic fields of 28 and 63 μG for two of the H I layers, at a reduced angular resolution of 100″. It is concluded that the magnetic field strength and the total pressure in the dense PDR are higher than in the more tenuous cloud envelope. However, in the cloud envelope the pressure is dominated by the magnetic field, while in the PDR turbulent pressure dominates.

Subject headings: ISM: individual (Orion B) — ISM: magnetic fields — ISM: structure — H II regions — radio lines: ISM

1. INTRODUCTION

1.1. H I *Observations of Photodissociation Regions*

The photodissociation of molecular hydrogen by UV photons in the wavelength range from 912 to 1108 Å is believed to play an important role in several astrophysical situations. The most obvious (and observationally best documented) situation where this process plays a role is the case of a molecular cloud bounding an H II region. The UV radiation that escapes from the ionization front longwards of the Lyman limit is absorbed by H_2 molecules in the Lyman and Werner electronic bands. In the following radiative cascade there is an 11% chance of dissociation. In the remaining 89% of the cases the molecule returns to the ground state, after emission of UV and infrared line photons. In the same region photodissociation of CO occurs, followed by rapid ionization of the atomic carbon that is produced. Thus the resulting *photodissociation region* or *photon-dominated region* (PDR) can be observed in the following ways:

1. By observing the fine-structure lines of [C II] at 158 μm and [O I] at 63 μm. These lines are the most important cooling lines of dense, warm PDRs (e.g., Tielens & Hollenbach 1985; Burton, Hollenbach, & Tielens 1990).

2. By observing rovibrational lines of H_2. These lines are emitted by H_2 molecules that do not dissociate after the initial electronic excitation, but cascade back to the ground state; in low-density gas ($n < 10^4$ cm^{-3}) a characteristic *fluorescent* spectrum results (Black & Van Dishoeck 1987; Sternberg 1988), while in higher density regions a more nearly thermal spectrum is produced (Sternberg & Dalgarno 1989).

3. By observing the H I 21 cm line from the dissociated gas.

These lines have been widely observed in galactic PDRs near O and early B stars (e.g., [C II] and [O I] lines: Russell et al. 1981; Crawford et al. 1986; Stutzki et al. 1988; Lane et al. 1990; Howe et al. 1991; H_2 rovibrational lines: Hayashi et al. 1985; Gatley et al. 1987; H I 21 cm line: Roger & Irwin 1982; Dewdney & Roger 1982, 1986; van der Werf & Goss 1989, 1990a, b), but observations of these types have also indicated the importance of photodissociation in more complicated situations. For instance, Stacey et al. (1991) obtained [C II] 158 μm spectra of a sample of galactic nuclei, and combined their measurements with existing H I data. These authors suggest that in

starburst nuclei a significant fraction (up to 40%) of the total gas mass is located in PDRs, and that much of the observed H I emission originates in these regions. Another indication for the importance of the large-scale photodissociation of H_2 has been presented by Allen, Atherton, & Tilanus (1986) and Tilanus & Allen (1989), who conclude that up to 20% of the H I in the disks of the spiral galaxies M83 and M51 may result from photodissociation. These various results suggest a crucial role for the photodissociation process in governing the H I/H_2 balance not only in star-forming molecular clouds, but also in galactic nuclei and galactic disks. In order to place this conclusion on firmer ground, it is of great importance to obtain a *quantitative* understanding of the H I production of a PDR.

Our current understanding of the H I content of PDRs is based on H I emission and H I absorption observations, which yield different types of information. H I *emission* studies of H II regions (e.g., Read 1981; Roger & Irwin 1982; Dewdney & Roger 1982, 1986) show the presence of extended layers of H I, containing typically a few hundred solar masses of atomic material, around the H II regions. The main limitation of these studies is confusion with unrelated H I clouds. In addition, there is the problem of distinguishing photodissociated H I from H I physically associated with the star-forming cloud, but not originating from photodissociation. H I *absorption* studies do not suffer from these problems. In the first place the confusion problem is greatly alleviated in absorption studies, and in the second place absorption studies toward bright continuum sources can yield high S/N ratios. These advantages, combined with the fact that the lines observed in absorption are generally narrower than those observed in emission, enable in many cases an analysis of the kinematic structure, which can then be used to distinguish between PDR and non-PDR H I (e.g., van der Werf & Goss 1989, hereafter Paper I). However, H I absorption observations of PDRs have the disadvantage that they cannot be used to determine the total amount of H I in a PDR, because only a fraction of the entire PDR is sampled by absorption measurements. Furthermore, the determination of H I column densities and masses from absorption data relies on the uncertain assumption of a temperature of the absorbing H I.

The temperature of the PDR gas is a source of some debate for another reason as well. Combinations of far-infrared fine-structure lines (e.g., the [C II] 158 μm line and the [O I] 63 μm and 145 μm lines; see, e.g., Watson 1984; Genzel, Harris, & Stutzki 1989) yield temperatures of several hundred degrees for the emitting gas. The H I emission observations do not directly measure temperature, but are consistent with a temperature of about 200 K and optically thin emission (e.g., Roger & Irwin 1982) in the PDR H I. Numerical models of PDRs (e.g., Tielens & Hollenbach 1985; Burton et al. 1990) yield similar temperatures. However, the H I absorption measurements yield a temperature constraint that is typically $T_s < 50$ K (Paper I; van der Werf & Goss 1990a, hereafter Paper II). However, at such low temperatures [C II] line emission is inefficient, since the upper level involved in this transition is 92 K above the ground state. For the O I transitions the situation is even more severe. This apparent contradiction must be resolved before a useful comparison between H I and other PDR lines (in the first place the [C II] 158 μm line) can be made.

In this paper H I observations of the galactic H II region Orion B are presented. The most important issues that will be addressed are the relation of the H I emission and absorption to the [C II] 158 μm emission and the temperature structure of the PDR. Furthermore, the average line-of-sight magnetic field in the absorbing H I will be determined. Before turning to the observations (§ 2), a brief summary of the most relevant properties of the Orion B complex is presented in § 1.2. Section 3 presents the results. In § 4 the H I and magnetic field results are interpreted and combined with other data, and a possible physical model to account for the observations is suggested. The conclusions are summarized in § 5.

1.2. *The Orion B Complex*

The galactic radio source Orion B (NGC 2024, W12, G206.5−16.4) is the second most prominent H II region in the Orion complex, located about 15′ east of the bright star ζ Ori, the easternmost star of the belt of Orion. This nebula has been the subject of considerable study at wavelengths ranging from the optical to the radio spectral region. Goudis (1982) has presented a review of early studies of Orion B and its environments. Orion B is located close to the southern tip of an elongated molecular cloud that measures about 5° from north to south and about 1° from east to west. This cloud is one of the two most prominent molecular clouds is a much larger complex of interstellar matter in Orion and Monoceros, that is centered at a galactic latitude of about −15°. An impressive overview of the complex is provided by the large-scale ^{12}CO $J = 1 \rightarrow 0$ map presented by Maddalena et al. (1986) and the *IRAS* 100 μm map published by Bally, Langer, & Liu (1991). The latter authors also provide a ^{13}CO $J = 1 \rightarrow 0$ map of the two main molecular complexes in Orion at a resolution of 100″. Maps of ^{12}CO $J = 1 \rightarrow 0$ (Stark & Bally 1982) and CS $J = 2 \rightarrow 1$ (Lada, Bally, & Stark 1991a), with a similar resolution are available as well. The large-scale distribution of H I in the complex has been mapped by Chromey, Elmegreen, & Elmegreen (1989) and (with better sampling) by Green (1991). The former authors find that the masses of atomic and molecular material in the complex are approximately equal.

Our understanding of the immediate surroundings of Orion B is reviewed by Barnes et al. (1989, hereafter BCBSW). Orion B is optically characterized by extended nebular emission that is partly obscured by a conspicuous, elongated dust lane, that crosses the emission nebula from south to north (see, e.g., BCBSW, their Fig. 8*a*). Spectral line and continuum observations in the millimeter and radio regimes have yielded a detailed picture of Orion B and its environments, which is described in detail in BCBSW, and briefly summarized below.

The bulk of the molecular gas and dust associated with Orion B is located behind the H II region. This gas is observed through the line emission of density tracing molecules, including CS, H_2CO, and HCN (see the multitransition studies by Snell et al. 1984; Evans et al. 1987; Mundy et al. 1987, all with an angular resolution of ∼1′), at an LSR velocity of approximately 11 km s^{-1}. Typical densities of 10^6 cm^{-3} are found in the background cloud. Graf et al. (1990, 1993) present measurements of low and mid-J lines of various CO isotopes and conclude that the background cloud contains a large (∼10^{23} cm^{-2}) column density of warm (∼100 K) gas. The CO $J = 7 \rightarrow 6$ image presented by Graf et al. (1993) shows structural features of both the H II region and the background cloud. Thus the warm gas is most likely located at the front surface of the background cloud, probably in a PDR immediately outside the ionization front on the far side of the H II region.

The dust lane in front of the H II region has been observed in absorption lines of H I (Lockhart & Goss 1978, hereafter LG), OH (Goss et al. 1976; BCBSW), and H_2CO (Bieging, Wilson,

& Downes 1982; Crutcher et al. 1986) and has an LSR velocity of about 9.5 km s^{-1}. This velocity component is also detected in low-J lines of various CO isotopes (Graf et al. 1993), but not in mid-J lines or in lines of density-tracing molecules, indicating that densities in the dust lane are lower than in the background molecular cloud. The dust lane is connected to the main molecular cloud behind the H II region through a tongue of molecular material that impedes the expansion of the H II region toward the south and explains the presence of the sharp ionization front at the southern edge of the H II region (BCBSW; Gaume, Johnston, & Wilson 1992; see also Grasdalen 1974). This molecular feature has been observed in HCO (Schenewerk et al. 1988), HCO^+ (Barnes & Crutcher 1990), NH_3 (Gaume et al. 1992), and low-J CO lines (Graf et al. 1993), and is intermediate in density ($n \sim 10^5$ cm^{-3}) and velocity ($v_{LSR} \sim 10$ km s^{-1}) between the background molecular cloud and the dust lane. The projected position of the luminous and dense molecular outflow in the Orion B complex is also located in this region (Sanders & Willner 1985; Russell, Hills, & Padman 1987; Richer et al. 1989; Barnes & Crutcher 1990).

The Orion B H II region itself has an LSR velocity of about 7 km s^{-1}, as determined from recombination lines of hydrogen and helium (Goudis 1982 and references therein; Krügel et al. 1982; Anantharamaiah, Goss, & Dewdney 1990). The ionized gas is thus flowing away from the background molecular cloud, which is at $v_{LSR} \approx 11$ km s^{-1}. Owing to the obscuration of the core of the H II region by the dust lane ($A_V \sim 30$ mag; Grasdalen 1974; Crutcher et al. 1986) the exciting star of the H II region has to date not been identified. The excitation of the H II region requires at least an O9.5 ZAMS star (see § 4.1). The closest O9.5 star is ζ Ori, but radio images show that this star is not well placed to account for the ionizing radiation, as had originally been thought (e.g., Hubble 1922). The most prominent near-IR source, NGC 2024–IRS 2, discovered by Grasdalen (1974), is a B0.5 ZAMS star and thus cannot account for ionizing radiation (Thompson, Thronson, & Campbell 1981). Lada et al. (1991b) find more than 100 sources with K magnitudes less than 13.0 in the H II region core (a near-IR image of these results is presented in Gillett & Houck 1991), but collective ionization by this cluster, as suggested by BCBSW and Lada et al. (1991b), has the problem of accounting for the strength of the observed helium recombination line emission. Radio and far-infrared morphology (Thronson et al. 1984) suggest that the exciting star is located about 30″ south of IRS 2, but this region contains no obvious candidate sources.

PDR emission from Orion B has been detected in all of the three ways listed in § 1.1. The [C II] $^2P_{3/2} \rightarrow {}^2P_{1/2}$ 158 μm fine structure line was first detected by Russell et al. (1980) and subsequently measured by Kurtz et al. (1983). Orion B is one of the brightest [C II] sources in the galaxy. Jaffe et al. (1993) present a [C II] map of the entire NGC 2024/2023/Horsehead complex with about 1′ angular resolution. The presence of PDRs both in front of and behind the H II region is shown by observations of C II radio recombination lines (Pankonin et al. 1977), which originate in the partly ionized regions outside the ionization front. At high frequencies these lines have an LSR velocity of about 11.5 km s^{-1}, while at lower frequencies they are found at about 9 km s^{-1}. This behavior is due to the increasing importance of stimulated emission for the low-frequency lines, thus showing that the C II region at 9 km s^{-1} is located in front of the H II region, while the C II lines at 11.5 km s^{-1} originate behind the H II region. In addition, narrow hydrogen recombination lines have been detected from Orion B at about 9 km s^{-1} (Pankonin et al. 1977; Anantharamaiah et al. 1990). These so-called H^0-lines also originate in a partly ionized medium outside the ionization front. The derived temperature is a few hundred degrees (Pankonin et al. 1977), in agreement with typical PDR conditions.

H_2 vibrational emission has been imaged in the $v = 1 \rightarrow 0$ $S(1)$ line by BCBSW. The emission follows the sharp ionization front at the south side of the H II region, and thus probably originates in a PDR in this region. The H_2 surface brightness decreases spectacularly where the dust lane crosses the ionization front, a feature most likely due to extinction. BCBSW estimate an extinction of up to a factor 100, i.e., $A_K \sim 5.0$ mag.

H I absorption toward Orion B was observed in detail for the first time by LG with the Owens Valley interferometer, at an angular resolution of 2′ and a velocity resolution of 0.84 km s^{-1}. They found three velocity components in the absorbing H I, at LSR velocities of 7.5, 9.5, and 11 km s^{-1}. Typical H I optical depths at the line centers were around 2, but at some positions exceeded 5. Chromey et al. (1989) found a pronounced unresolved (with their 20′ beam) H I peak at the position of Orion B, which they attribute to H I in the PDR. This H I has a column density of $\sim 3 \times 10^{21}$ cm^{-2}, average H I density ~ 600 cm^{-3}, and a total H I mass of about 100 $M_\odot$.

The line-of-sight component $B_\parallel$ of the magnetic field in front of Orion B has been determined from circular polarization observations of the Zeeman components of the OH hyperfine lines at 1665 and 1667 MHz (Crutcher & Kazès 1983; Kazès & Crutcher 1986; Heiles & Stevens 1986). The resulting value for $B_\parallel$ is $+38$ μG, with the usual sign convention that a positive value of $B_\parallel$ indicates that the field lines are pointing away from the observer (note that the Crutcher & Kazès 1983 detection paper incorrectly gave the sign of $B_\parallel$ as negative).

The distance to Orion B is 415 pc, as derived by Anthony-Twarog (1982) from Strömgren photometry of the associated star cluster. At this distance, 1′ corresponds to 0.12 pc.

2. OBSERVATIONS AND REDUCTION

H I 1420 MHz observations of Orion B were carried out in 1984 October using the Very Large Array (VLA, Thompson et al. 1980) of NRAO in the D-configuration. Observational parameters are summarized in Table 1. Using the frontend switches, right-hand (R) and left-hand (L) circular polarization were observed alternately for 4 minute intervals. Thus at every moment, only R or L was recorded (in contrast to the present situation at the VLA, where R and L can be recorded simultaneously). Short observations of the amplitude and phase calibration source were carried out every hour. All calibration sources were observed at frequencies displaced 1 MHz (~ 200 km s^{-1}) from the observing frequency for Orion B, in order to avoid the effects of H I emission on the phases of the amplitude and phase calibrator, and of H I absorption in the flux density and passband calibrators. In order to avoid frequency-dependent effects, both positive and negative frequency shifts were applied, and the corresponding calibration measurements were averaged. The flux density calibration is based on the scale of Baars et al. (1977). After editing of the data, correction for shadowing, and calibration the visibility data were interpolated to a square uv-grid and Fourier transformed, to yield two sets (one for R, one for L) of 31 images of the flux density distribution of Orion B at different velocities v_{LSR}.

TABLE 1

OBSERVATIONAL PARAMETERS

Parameter	Value
Right ascension of field center	$5^h39^m13^s.6$ (1950.0)
Declination of field center	$-1°55'57''$ (1950.0)
Observation date	1984 Oct 30
Total observing time	11 hr
Configuration	D-array
Number of antennas	25
Polarization	R and L circular (recorded separately)
Calibration sources:	
Flux density calibrator	3C 147 (22.2 Jy)
Amplitude and phase calibrator	0500+019 (2.51 Jy)
Passband calibrator	3C 48
Shortest baseline observed	33 m
Longest baseline observed	1030 m
FWHM of primary beam	30′
Beam major axis (FWHM)	49″.8
Beam minor axis (FWHM)	40″.3
Position angle of beam major axis	170°
Central velocity of observation	10.0 km s^{-1} (LSR)
Total bandwidth	94.60 kHz 19.96 km s^{-1}
Channel spacing	3.0516 kHz 0.644 km s^{-1}
Velocity resolution	0.644 km s^{-1}
Rms noise	
Clean continuum	4.7 mJy beam^{-1} (1.4 K)
Clean line channels	9 mJy beam^{-1} (2.7 K)
Conversion factor	0.304 K (mJy beam^{-1})$^{-1}$

Subsequent data reduction was carried out using the Groningen Image Processing System (GIPSY; Allen, Ekers, & Terlouw 1985). First the R and L data sets were converted to Stokes parameter data $I = (R + L)/2$ (total intensity) and $V = (R - L)/2$ (circular polarization). The V data set was found to contain a small contribution (about 3.5% over the entire source) of I signal, due to the gain difference of the R and L channels. This contribution was removed in the manner described by Troland, Heiles, & Goss (1989), yielding a true Stokes V data set.

Significant positive and negative sidelobes were present in the synthesized antenna pattern. The negative sidelobes created a pronounced negative "bowl" around Orion B in the Stokes I data. Therefore these maps were cleaned using a procedure especially suited for the deconvolution of extended sources, the multiresolution CLEAN method (Wakker & Schwarz 1988). After this reduction step, the depth of the bowl was less than two times the rms noise. A continuum map was then created by averaging nine line-free channels at velocities smaller than 2.9 and larger than 16.4 km s^{-1}. The resulting (deconvolved) images were then corrected for attenuation due to the VLA primary beam.

In order to compute the H I opacities from the line and continuum images, the equation of transfer given in Paper I must be solved. This equation can be inverted directly if $|T_s - T_{bg}(v)| \ll T_c$, where T_s is the spin temperature of the absorbing H I, $T_{bg}(v)$ is the brightness temperature of the background H I at velocity v, and T_c is the continuum brightness temperature. The H I emission in the Orion B area has typically a 70 K peak brightness temperature (Green 1991), and this value provides an upper limit to $T_{bg}(v)$. Values for T_s are typically of the order of 50 K, so that $|T_s - T_{bg}(v)|$ will be typically a few tens of K. The calculation of the opacities was therefore restricted to areas where $T_c > 100$ K, which is about 6% of the peak value. At this continuum level the minimum opacity that can be detected is about 0.1, while the maximum detectable opacity before saturation limits the precision is about 3. Typical errors in the derived opacities are a few tens of percents in these regions. However, over most of the source the uncertainty in the opacity is only a few percent, with minimum and maximum detectable opacities of about 0.01 and 5.

For the analysis of the Zeeman effect the uncleaned data sets were used. The S/N ratio in the full resolution data was insufficient, and became satisfactory only after smoothing to a 100″ circular beam. At this resolution, all structural information about the magnetic field is lost, and only an average value, pertaining to a 100″ FWHM area, centered on the continuum peak, could be derived.

3. RESULTS

3.1. *Continuum*

The cleaned 21 cm continuum image showing the thermal radio emission from the Orion B H II region is presented in Figure 1. The rms noise in this image is 4.7 mJy beam^{-1} and the total flux is 65 Jy, in agreement with previous measurements with single dishes (Pauliny-Toth, Wade, & Heeschen 1966; Terzian, Mezger, & Schraml 1968) and aperture synthesis instruments (LG; Löbert & Goss 1978). The overall morphology, characterized by the mainly east–west orientation of the brighter areas of radio emission and the sharp ionization front on the south side of the H II region are in agreement with existing radio images. The faint extended emission to the north side of the H II region core has also been observed at a frequency of 330 MHz by Subrahmanyan (1991), who interprets this feature as a radio jet. However, the counterjet detected by Subrahmanyan south of the H II region is not found in the present data.

3.2. H I *Absorption*

The velocity structure of the absorbing H I is illustrated by the H I opacity spectrum shown in Figure 2. This spectrum clearly shows the three velocity components also found by LG. The spectrum is well fitted by three Gaussian components. The data were further processed by fitting three-component Gaussian profiles to all the opacity spectra. This procedure yielded maps of peak opacity τ_0, central velocity v_0, and velocity FWHM Δv for each of the three absorbing components. The τ_0 and Δv images were combined to yield images of $N(\text{H I})/T_s$. Global properties of the three components were derived from these images and are presented in Table 2. A typical spin temperature $T_s = 25$ K is adopted for the absorbing H I, based on the fact that H I absorption is seen even toward regions with a continuum brightness temperature of $\lesssim 20$ to 30 K. The use of this temperature in analyzing the H I absorption data will be justified in § 4.2.4. Following Paper I, the absorbing H I components are labeled A, B, and C in order of decreasing central velocity. As pointed out in § 1.1, the calculated H I masses are only a lower limit, since only part of the H I associated with the H II region is seen in absorption, and since only the cold gas component absorbs efficiently. A comparison with the results of LG shows good agreement of the average peak opacities and central velocities, but LG derive line widths that are about 50% larger than the line widths found in the present work. The H I column densities and mass limits derived by LG are (after

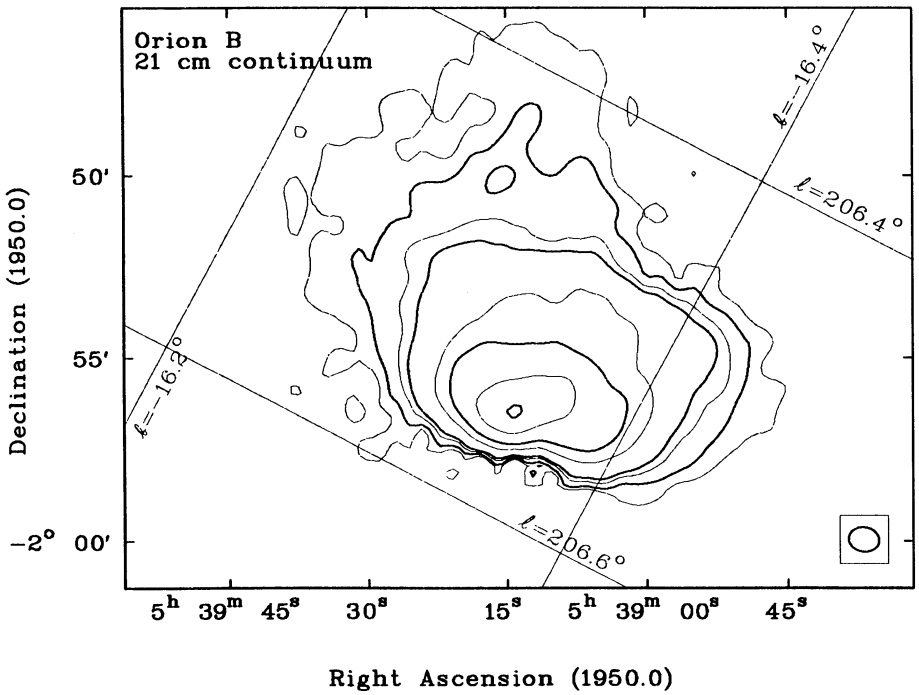

FIG. 1.—Cleaned 21 cm continuum image of Orion B. Contours alternate in thickness and correspond to 25, 50, 100, 150, 500, 1000, 2500, and 5000 mJy beam^{-1}.

accounting for the difference in the adopted spin temperature) correspondingly higher. Images of N(H I)/T_s in components A, B, and C are presented in Figures 3, 4, and 5*a*. Figure 5*b* shows the velocity field of component C. The remaining velocity fields and the line width maps are generally featureless and are not shown here. Considering the difference in angular resolution, the results are in agreement with the results obtained by LG, except for the velocity gradient in component B found by LG, which is not found in the present data.

3.3. H I *Emission*

Careful inspection of individual channel maps and spectra revealed the presence of H I *emission* in addition to the three absorption components. The emission is found only at velocities redshifted with respect to the absorption lines. Figure 6

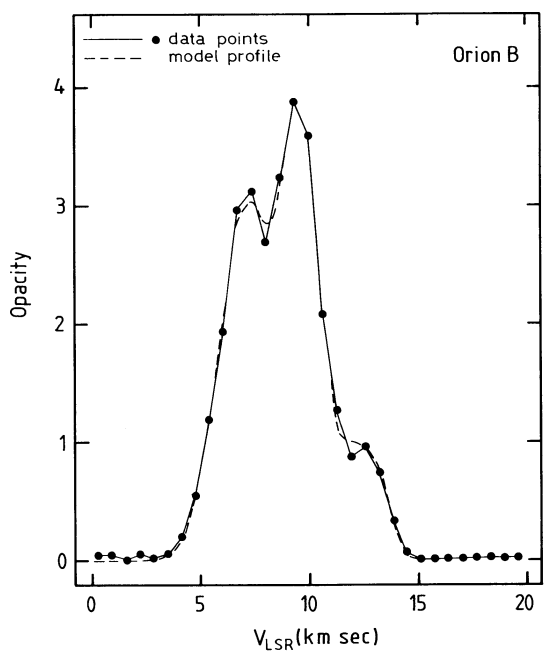

FIG. 2.—Spectrum of H I optical depth toward the core of the Orion B H II region. This spectrum has been constructed by computing a weighted average over a 70″ × 60″ (east × west) area centered on the continuum peak (R.A. = 5^{h}39^{m}17^s.0, decl. = −1°54′57″), using the background continuum brightness temperature as weighting factor. The dashed line shows a three-component Gaussian model profile that has been fitted to the spectrum.

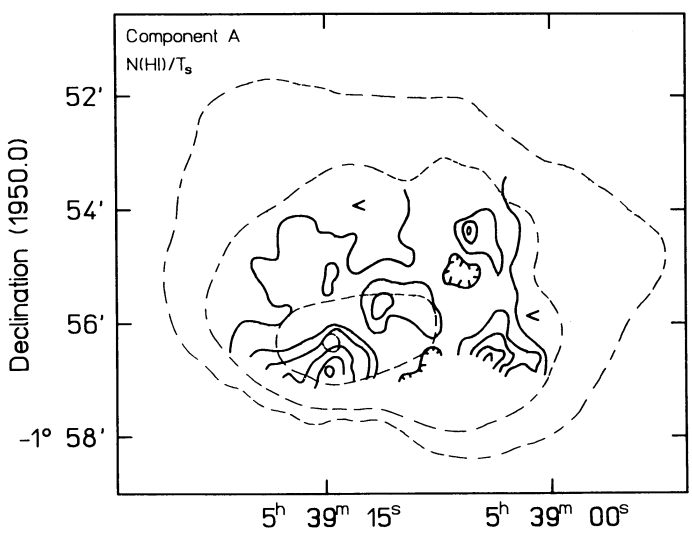

FIG. 3.—The distribution of N(H I)/T_s in H I component A, shown by solid contours drawn at values of 1, 2, 3, 4, 5, and 6 × 10^{19} cm^{-2} K^{-1}, overlaid on continuum contours (*dashed*) drawn at 150, 500, 2500, 5000 mJy beam^{-1}.

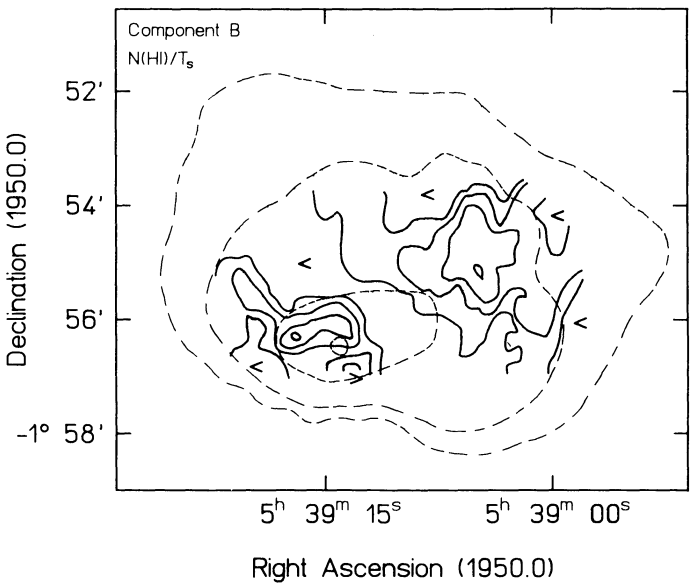

FIG. 4.—As Fig. 3, but for H I component B, and with solid contours drawn at values of 3, 6, 9, and 12 × 10^{19} cm^{-2} K^{-1}.

shows an individual H I channel map at v_{LSR} = 15.8 km s^{-1}, showing the presence of H I emission as well as absorption at this velocity. The H I emission peaks at the southern edge of the H II region, close to the edge-on ionization front. In Figure 7 a spectrum averaged over the region of strongest H I emission is shown. The spectrum shows that only the red wing of the H I emission line is observed. Strong absorption by the foreground H I component A precludes detection of the peak of the emission line, which is estimated to be located at a velocity of ~12–13 km s^{-1}. This result implies that peak brightness temperatures in this emission line must be considerable, since brightness temperatures in excess of 60 K are already reached in the line wings. Because of the lack of information on the shortest interferometer baselines, the images are deficient in structures larger than about 9′. The bright H I emission features detected here are clearly small compared to this scale.

TABLE 2

GLOBAL PROPERTIES OF THE ABSORBING H I COMPONENTS

Property	A	B	C	Notes
τ_0	1.0	3.8	3.1	
v_0 (km s^{-1})	12.1	9.6	6.6	
Δv (km s^{-1})	2.2	2.5	2.9	
N(H I)/(T_s/25 K) (cm^{-2})	1.0 × 10^{20}	4.6 × 10^{20}	4.3 × 10^{20}	a
M(H I)/(T_s/25 K) ($M_\odot$)	0.25	2.5	2.3	a, b
$B_\parallel$ (μG)	28	38	63	c
f(%)	>2	>1.3	>25	d
p_{th} (cm^{-3} K)	2 × 10^4	2 × 10^5	2 × 10^6	e
p_{turb} (cm^{-3} K)	1 × 10^5	5 × 10^6	5 × 10^7	e
p_{mag} (cm^{-3} K)	2 × $10^5 x^2$	4 × $10^5 x^2$	1 × $10^6 x^2$	e

[a] Using a distance of 415 pc (Anthony-Twarog 1982).
[b] Lower limits to mass of absorbing H I.
[c] Value for component B from OH (Kazès & Crutcher 1986; Heiles & Stevens 1986).
[d] Atomic fractions (see § 4.2.2) for T_s = 25 K.
[e] See text, § 4.3.

3.4. *Magnetic Field*

The only statistically significant Stokes V signal in the 100″ resolution data set is found at the continuum peak, at velocities of 6.1 and 14.5 km s^{-1}. The relevant I and V spectra are shown in Figure 8. The line-of-sight component of the magnetic field was derived by dividing the observed V signal by the velocity derivative of I, yielding $B_\parallel$ = 63 ± 8 μG at v_{LSR} = 6.1 km s^{-1} and $B_\parallel$ = 28 ± 8 μG at v_{LSR} = 14.5 km s^{-1}. The value $B_\parallel$ = 38 μG derived from OH measurements (Crutcher & Kazès 1983; Kazès & Crutcher 1986; Heiles & Stevens 1986) lies between those two values and has the same sign. It should be noted that the value derived at 14.5 km s^{-1} applies to H I

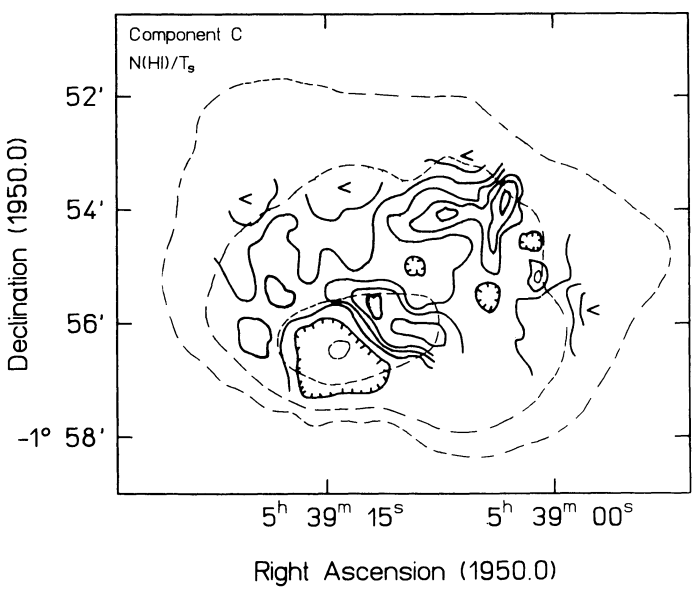

FIG. 5a

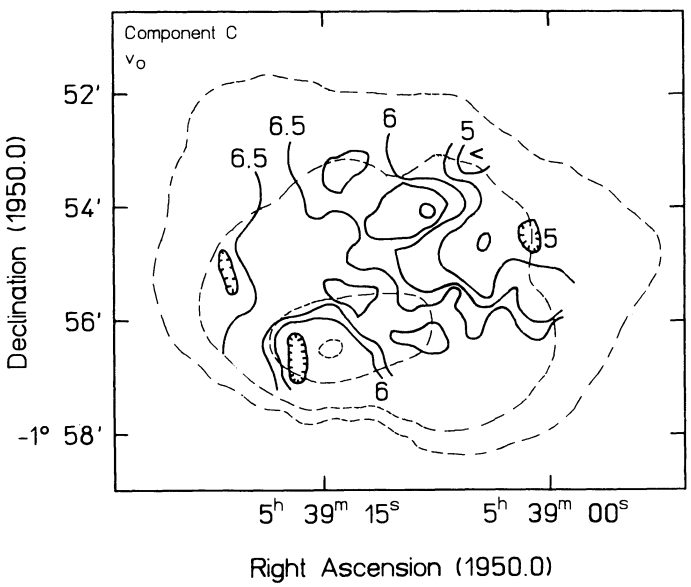

FIG. 5b

FIG. 5.—(*a*) As Fig. 3, but for H I component C, and with solid contours drawn at values of 2, 4, 6, 8, 10, and 12 × 10^{19} cm^{-2} K^{-1}. (*b*) As Fig. 5*a*, but now the central velocity of H I component C is shown by the solid contours, drawn at 5.0, 5.5, 6.0, 6.5, and 7.0 km s^{-1}.

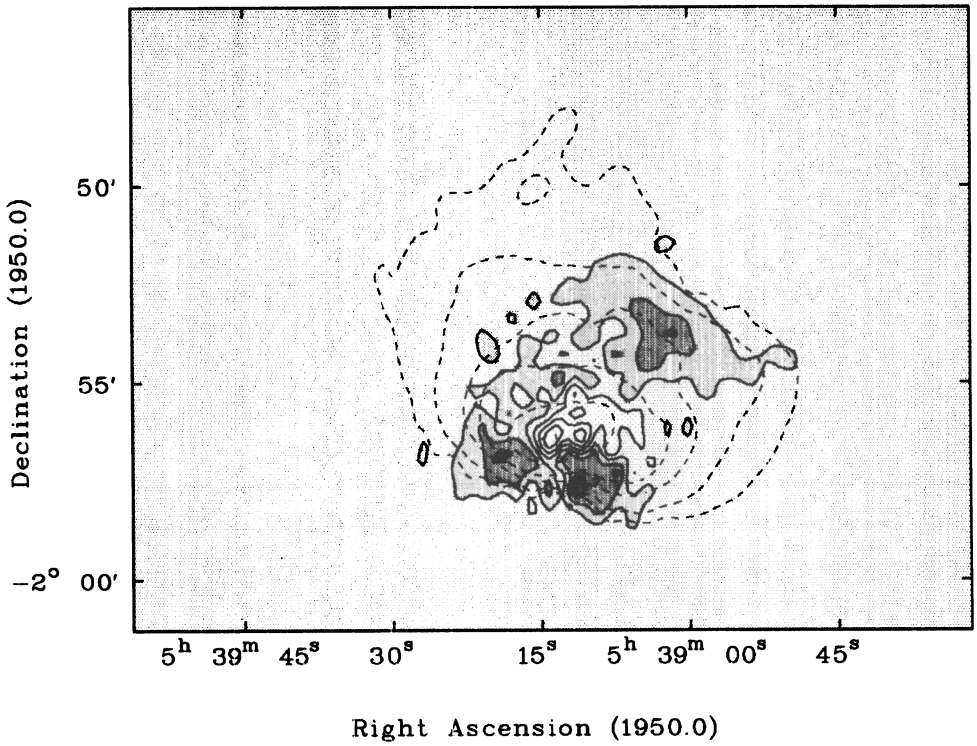

FIG. 6.—H I emission and absorption brightness temperature at $v_{LSR} = 15.8$ km s^{-1}, denoted by the solid contours and the gray scale. Low brightness temperatures in either emission or absorption (i.e., $|T_b| < 10$ K) are denoted by the light gray that fills most of the image. Lighter shades of gray denote H I *absorption*, darker shades H I *emission* of more than 10 K at this velocity. Gray-scale transitions (marked by solid contours) from light to dark are at -50, -30, -10, 10, 30, and 50 K. The 21 cm continuum is indicated by the dashed contours (contour levels at 50, 150, 500, 1000, 2500, and 5000 mJy beam^{-1}).

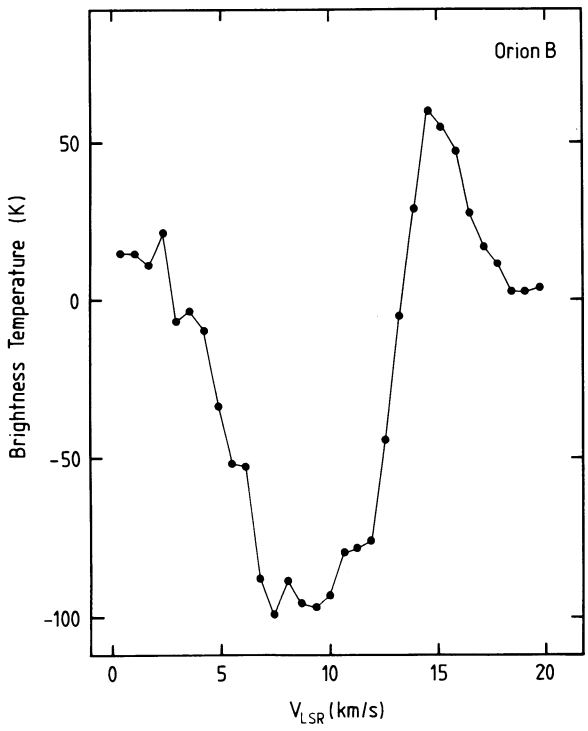

FIG. 7.—Average H I spectrum over a 40″ square area centered at R.A. 5h39m10s.3, Decl. −1°57′37″, i.e., the region of strongest H I emission in Fig. 6.

component A, while the value derived at 6.1 km s^{-1} is relevant to H I component C. In both these components, only the line wing that does not overlap with the strongly absorbing component B shows detectable circular polarization. There is no circular polarization detected from component B in the present data, due to overlap of the line wings with components A and C. However, the OH measurements apply to material at $v_{LSR} = 9$ km s^{-1} (Heiles & Stevens 1986), corresponding to H I component B in the present data, and thus presumably measure the line-of-sight magnetic field in component B.

4. DISCUSSION

4.1. *Continuum*

The maximum brightness temperature of the thermal continuum of the H II region is found to be 1600 K. Assuming an electron temperature of 8000 K (see references in Goudis 1982), the implied continuum optical depth of the H II region at the continuum peak is 0.22, and the peak emission measure $E = 1.1 \times 10^6$ pc cm^{-6}, in agreement with previous measurements (e.g., Löbert & Goss 1978). Thus the H II region is essentially optically thin over most of its area. The faint north-east "halo" of the H II region has typically $E = 4.3 \times 10^4$ pc cm^{-6}. Using typical sizes of 5′ for both H II region core and halo as pathlengths (corresponding to 0.6 pc at the assumed distance of 415 pc), average rms electron densities are $n_{e,rms} = 1300$ cm^{-3} in the core and $n_{e,rms} = 250$ cm^{-3} in the halo. The excitation parameter of the H II region $u = 30$ pc cm^{-2}, in agreement with previous measurements (see references in Goudis 1982). The required Lyman continuum photon flux for an ionization bounded, dust-free H II region with this value of u is

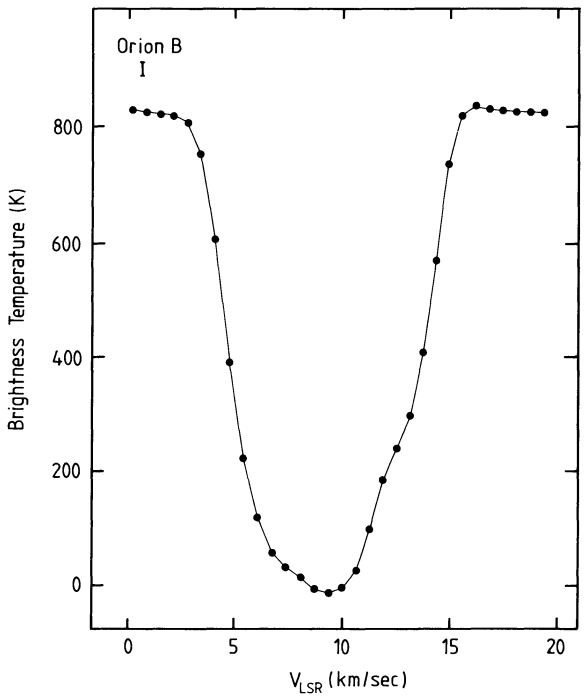

FIG. 8a

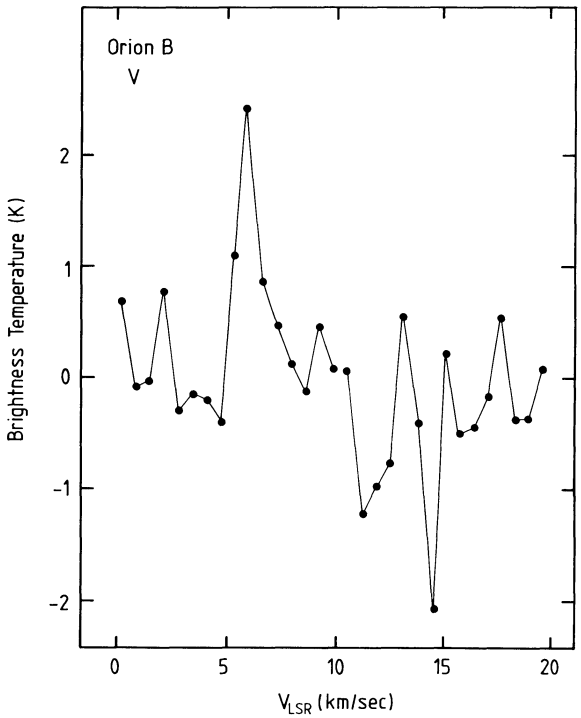

FIG. 8b

FIG. 8.—(*a*) Stokes *I* spectrum at 100″ resolution at the continuum peak. (*b*) Corresponding Stokes *V* spectrum.

$N_{Lyc} = 1.2 \times 10^{48}$ s^{-1}. The ionization of the H II region thus requires at least an O9 ZAMS or O9.5 V star (Panagia 1973).

4.2. *Properties of the Atomic Gas*

4.2.1. *Velocity Structure and Geometry*

In Paper I a model for the H I in front of Orion A was developed to explain the threefold velocity structure visible in absorption. The same model was shown to apply to several of the compact H II regions in W3 (Paper II). An analysis of velocity agreements of the present H I data with other lines leads to an essentially identical model for the H I in front of Orion B. The proposed geometry is illustrated in Figure 9. The arguments that support this picture are given below.

The H I absorption data are most usefully compared with other absorption data, since such measurements sample only material in front of the H II region. The most pronounced molecular absorption lines occur at $v_{LSR} \approx 9.5$ km s^{-1}, e.g., OH measurements by Goss et al. (1976), Crutcher & Kazès (1983), and BCBSW, and H_2CO measurements by Bieging et al. (1982). This material agrees in velocity with H I component B in the present data and corresponds to the optical dust lane in front of the H II region (cf. § 1.2). The structural features of N(H I)/T_s in component B (Fig. 4) agree roughly with those seen in OH absorption at the same velocity (BCBSW). The molecular absorption studies referred to above also show the presence of a secondary, less opaque absorption feature at $v_{LSR} \approx 12$ km s^{-1}, i.e., at the velocity of H I component A and the bulk of the molecular gas. The higher opacity of the 9 km s^{-1} component compared to the 12 km s^{-1} component in the molecular absorption lines is also found in the present H I data.

No molecular counterpart to H I component C at 6.6 km s^{-1} has been detected. However, this H I component agrees in velocity with the ionized gas, as is shown by a comparison with hydrogen radio recombination line observations (e.g., Krügel et al. 1982). Furthermore, component C also shows features of the continuum, unlike the other two H I components. The most obvious feature is the local minimum of N(H I)/T_s at the continuum peak, which is bordered by a ridge of enhanced N(H I)/T_s (Fig. 5*a*). At the position of the minimum in N(H I)/T_s, the central velocity of component C also shifts to lower values (Fig. 5*b*). The agreement in position and velocity with the continuum peak suggests a close proximity of component C to the ionized gas. This feature thus probably originates in the PDR in front of the H I region. The

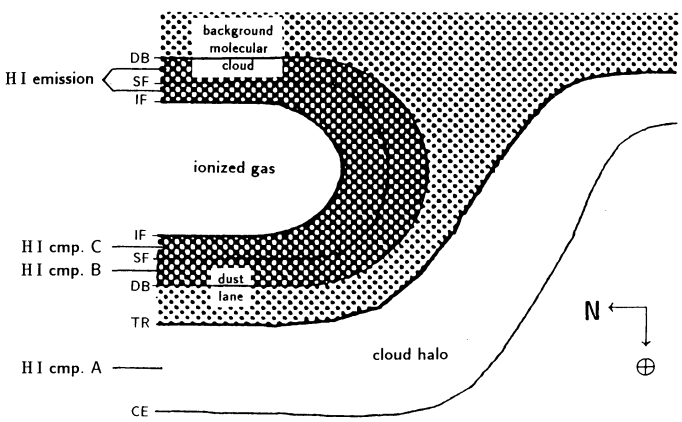

FIG. 9.—Schematic representation of the proposed physical model for the environment of Orion B, showing the positions of the various H I components. Molecular gas is shaded light, while photodissociation regions are shaded dark. The abbreviations have the following meanings: IF: ionization front; SF: shock front; DB: dissociation boundary; TR: transition to cloud halo; CE: cloud edge.

agreement in velocity with the ionized gas is then due to the fact that this H I layer has been passed by the shock front that precedes the ionization front (Lasker 1966; Spitzer 1978). This H I component thus plays exactly the same role as component C in front of Orion A (Paper I).

H I components A and B are located farther from the H II region. Since the molecular feature that impedes the expansion of the H II region toward the south (and thus is located close to the ionized gas) is connected to the dust lane (Barnes & Crutcher 1990), the dust lane itself is located close to the front side of the H II region. Thus the associated H I component B is probably located directly in front of component C. The radiation escaping from the H II region longwards of the Lyman limit has created a PDR at the side of the dust lane facing the H II region, as shown by the presence of carbon radio recombination lines at ~ 9 km s^{-1} from in front of the H II region (Pankonin et al. 1977; Anantharamaiah et al. 1990). The atomic gas in this PDR is observed as H I component B. Part of this PDR has been overtaken by the shock front in front of the ionization front, which gives rise to a kinematically distinct feature, observed here as H I component C. Assuming that the temperatures of components B and C are approximately equal, the column densities of shocked (component C) and unshocked (component B) PDR gas are similar. The proportion of shocked to unshocked H I in a PDR is investigated theoretically by Roger & Dewdney (1992, their Fig. 14). In their highest density model ($n = 3000$ cm^{-3}), equal column densities of shocked and unshocked H I are reached after a few times 10^5 yr, in agreement with the estimated dynamical age of Orion B (Gordon 1969; Grasdalen 1974).

Turning finally to H I component A, the detection of H I and faint molecular absorption at the velocity of the background molecular cloud indicates that a minor part of the molecular cloud associated with Orion B must be located in *front* of the H II region instead of behind it. This geometry can be understood by noting that molecular clouds usually possess halos of more diffuse material, where the transition between molecular and atomic gas takes place (e.g., Elmegreen 1989; Chromey et al. 1989, and references therein). These halos act as shielding layers, protecting the deeper cloud layers from dissociating radiation. The thickness of these layers depends on radiation field, density, metallicity, and pressure, but can be typically a few pc (Federman, Glassgold, & Kwan 1979; Elmegreen 1989). Cromey et al. (1989) have demonstrated the presence of such shielding layers in the Orion B region. At the front side of the Orion B molecular cloud the shielding layer will extend in front of the H II region, and thus be observable in absorption. It is therefore concluded that component A originates in the diffuse halo of the background molecular cloud, extending in front of the H II region. Of the three H I components, this component is located farthest from the ionization front, in agreement with the absence of radio recombination lines from a partly ionized medium from this layer. The presently detected component A plays exactly the same role as component A in front of Orion A (Paper I).

In the following sections this model of the absorbing layers, which was constructed here on the basis of qualitative and plausibility arguments, will be further tested and placed on a more quantitative foundation.

4.2.2. *Atomic Fractions of the Absorbing* H I *Layers*

The atomic fractions $f = N(\text{H I})/[N(\text{H I}) + 2N(H_2)]$ in the H I components can be determined from a comparison with molecular absorption line data. Since such data refer mainly to component B, the analysis will focus on that component. The most useful approach is to consider the upper limit $N(H_2) < 8.8 \times 10^{22}$ cm^{-2} derived by Black & Willner (1984) from their nondetection of H_2 vibrational lines in absorption toward NGC 2024–IRS 2. At this position the H I column density in component B is $N(\text{H I}) = 2.3 \times 10^{21}(T_s/25\ \text{K})$ cm^{-2}, so that $f > 1.3\%$. For $T_s = 45$ K (as suggested by the CO $v = 2 \leftarrow 0$ absorption data presented by Black & Willner 1984), the result becomes $f > 2.3\%$. H_2 column densities derived from H_2CO and OH absorption measurements depend on assumptions regarding excitation temperatures and abundances, but are consistent with this result.

The atomic fractions for components A and C are best determined relative to component B. For component A the OH spectrum shown by BCBSW yields $\tau_0(1667) \approx 0.07$, while $\tau_0(\text{H I}) \approx 1$. Under the assumption that all other parameters are equal for components A and B, it follows that $f_{\text{cmp A}} \approx 1.5 f_{\text{cmp B}}$. For component C, $\tau_0(\text{H I}) \approx 3$, while $\tau_0(1667) < 0.015$ (BCBSW), resulting in $f_{\text{cmp C}} > 20 f_{\text{cmp B}}$. Although the OH abundance in PDRs may differ from the usual value in molecular clouds (the UV destruction rate of OH is enhanced in PDRs, but so is the OH formation rate due to the elevated gas temperature, e.g., Hartquist & Sternberg 1991), it is clear that a significant fraction of the gas in component C is in the form of H I, since no molecular lines have been observed from this velocity component.

The high atomic fraction of component C is obviously in agreement with its location in the PDR. The atomic fractions of the other two components, are, although much lower, still higher than typical molecular cloud values (e.g., van der Werf, Goss, & Vanden Bout 1988). In component B, the enhanced H I fraction is most likely due to enhanced photodissociation by the exciting stars of the Orion B H II region. The H I fraction in component A is typical for a molecular cloud envelope where shielding from the interstellar radiation field is diminished and H_2 reformation is slow due to lower densities than in the cloud interior (van der Werf et al. 1988, 1989).

4.2.3. *Location and Properties of the Emitting* H I

If the H I observed in emission (Figs. 6 and 7) is located in front of the H II region, the implied temperature is at least 750 K, or it would have been in absorption. This temperature is higher than temperatures estimated for PDRs from far-infrared fine structure lines and from radio recombination lines, which typically amount to 150 to 300 K, but is not ruled out by these measurements. Furthermore, numerical models of PDRs do predict the presence of a small amount (column density at most 10^{20} cm^{-2}) of hot ($T_s > 1000$ K) gas close to the ionization front, where H_2 vibrational heating is important (e.g., Burton et al. 1990). However, in view of its central velocity of about 12.5 km s^{-1}, it is much more likely that the H I emission is associated with the background molecular cloud, and thus originates behind the H II region, which is possible because the H II region is mostly optically thin at 21 cm (§ 4.1). The high brightness temperature of the H I emission and the fact that the brightest features are located near the southern ionization front, make a PDR origin of this emission very likely. This conclusion is supported further by morphological similarities of the H I emission to the [C II] 158 μm emission mapped by Jaffe et al. (1993).

The average H I emission brightness temperature at 15.8 km s^{-1} (Fig. 6) is 20 K (excluding the positions where absorp-

tion is found), but peak values exceed 60 K. These values refer to the wing of the emission line. From a comparison with single-dish measurements (Green 1991) it is estimated that brightness temperatures at the line center will be typically a factor of 3 higher. If the line is optically thin, the implied H I column density is then about 6×10^{20} cm^{-2} on average (estimating from Fig. 7 a line width of ~ 5 km s^{-1} FWHM), with peak values of about 2×10^{21} cm^{-2}. Chromey et al. (1989) found an H I concentration at the position of Orion B with a column density of 3.2×10^{21} cm^{-2}, at a resolution of 20′. Although the central velocity of that feature is uncertain, it appears that the column density of the emitting H I may even be substantially higher than estimated here.

4.2.4. *Combining* H I *Absorption and Emission*

PDR H I assciated with Orion B has been detected in absorption from a PDR in front of the H II region and in emission from a PDR behind the H II region. Some interesting conclusions concerning these regions can be derived under the assumption that these regions have similar physical properties. It is thus assumed that the H I emission line and the H I absorption from components B and C originate in regions that, apart from unimportant variations in density, temperature, and column density, have comparable physical structures and conditions.

This approach immediately implies that a *range of temperatures exists in the PDRs.* The presence of material colder than about 20 K is inferred from the presence of H I absorption at positions with continuum brightness temperatures of about 20 K, thus showing that at least a fraction of the H I is colder than 20 K. The emitting H I has a *minimum* spin temperature of ~ 50 K on average, but of ~ 200 K at the peak (as implied directly by the brightness temperatures). The actual spin temperature of the emitting H I may thus be in the range indicated by far-IR fine structure lines, i.e., $T \sim 250$ K. The H I emission from the background PDR is dominated by this *warm* H I. In contrast, the absorption data select only the coldest material. As a corollary, the analysis of the absorption data using a single low temperature (25 K in the present case) is justified. However, this conclusion also implies that the H I column densities determined in this way refer only to the cold component and may significantly underestimate total H I column densities if a range of temperatures is present.

4.2.5. *Combining* H I *and* [C II] 158 μm *Data*

After the considerations of the preceding section, the H I data can be combined with the [C II] 158 μm line data. Intensities $I_{[\mathrm{C\ II}]}$ are taken from Jaffe et al. (1993). In order to assess the relative contributions of foreground and background PDRs to the observed $I_{[\mathrm{C\ II}]}$ values, the velocity-resolved spectrum published by Betz, Boreiko, & Zmuidzinas (1990) is used. This spectrum shows two peaks: one at 12 km s^{-1} and one at 8 km s^{-1}. These velocities are in agreement with the average velocities of respectively the background and foreground PDRs. The possibility that the two peaks in the [C II] spectrum are produced by self-absorption, as suggested by Betz et al. (1990) is dismissed, since even lines that are completely optically thin (e.g., $^{13}C^{18}O$ $J = 2 \rightarrow 1$; Graf et al. 1993) show a double-peaked structure.

From the [C II] spectrum presented by Betz et al. (1990) it is concluded that on average $\sim \frac{1}{3}$ of the observed $I_{[\mathrm{C\ II}]}$ originates in the foreground PDR, while the remainder originates in the background PDR. Implied average surface brightnesses (in excess of more extended emission) from Jaffe et al. (1993) are then $I_{[\mathrm{C\ II}]} = 3.3 \times 10^{-4}$ erg s^{-1} cm^{-2} sr^{-1} for the background PDR and half of this amount for the foreground PDR. The contribution to the [C II] 158 μm line flux by the H II region is negligible, since a large fraction of the carbon within the H II region will be doubly ionized (Russell et al. 1980; Kurtz et al. 1983; Melnick et al. 1986). This conclusion is confirmed by the small line width of the 7.5 km s^{-1} component of the [C II] line.

The dependence of $I_{[\mathrm{C\ II}]}$ on physical parameters is given by

$$I_{[\mathrm{C\ II}]} = 4.7 \times 10^{-21} N([\mathrm{C\ II}]) \frac{e^{-91/T}}{1 + 2e^{-91/T} + n_{\mathrm{crit}}/n}, \quad (1)$$

with all quantities in cgs units (Crawford et al. 1985). The critical density $n_{\mathrm{crit}} \approx 0.79[T(\mathrm{K})]^{1/2}$ cm^{-3} for electron impact excitation (Haye & Nussbaumer 1984), $n_{\mathrm{crit}} = 3000$ cm^{-3} for excitation by collisions with hydrogen atoms (Launay & Roueff 1977), and $n_{\mathrm{crit}} = 5000$ cm^{-3} for collisions with H_2 (Flower & Launay 1977; Flower 1988). The latter two values are approximately independent of temperature between 60 and 1000 K. In the case of thermal emission ($n \gg n_{\mathrm{crit}}$) equation (1) reduces to

$$I_{[\mathrm{C\ II}]} = 1.4 \times 10^{-24} N(\mathrm{H\ I}) \frac{e^{-91/T}}{1 + 2e^{-91/T}}, \quad (2)$$

where the simplification has been made that in the PDRs all carbon (with [C]/[H] $= 3 \times 10^{-4}$, Cameron 1973) is singly ionized and all hydrogen atomic.

Application of this equation leads immediately to the conclusion that the cold H I dominating the absorption hardly contributes to the observed [C II] emission, since with $T = 25$ K, $I_{[\mathrm{C\ II}]} = 3.5 \times 10^{-26} N(\mathrm{H\ I})$. The observed H I column density at 25 K seen in absorption then produces an $I_{[\mathrm{C\ II}]} = 3.0 \times 10^{-5}$ erg s^{-1} cm^{-2} sr^{-1}, i.e., a factor of 5 less than the observed intensity. The observed [C II] 158 μm emission must therefore originate in the warmer component of the PDR. In order to test this interpretation, we consider the bright east–west elongated feature in the [C II] image published by Jaffe et al. (1993). For this feature, that probably originates in a PDR close to the southern edge-on ionization front, Jaffe et al. (1993) find $I_{[\mathrm{C\ II}]} \approx 1.4 \times 10^{-3}$ erg s^{-1} cm^{-2} sr^{-1}, corresponding to about 3×10^{21} cm^{-2} of warm material, in agreement with estimates from the bright H I emission. In the following, a two-temperature model is adopted. The lower temperature will be 25 K and the higher one can reach values of a few hundred degrees or more. Although a continuous range of temperatures may be physically more correct, a simple two-temperature model is probably the most sophisticated model warranted by the data.

The [C II] 158 μm intensities from the background and foreground PDRs correspond to warm column densities of about 8×10^{20} and 4×10^{20} cm^{-2} respectively. Thus the fraction of H I in the foreground PDR that is warm is approximately 30%. These numbers are relatively insensitive to the assumed temperature as long as the gas is at a temperature of a least a few hundred degrees. Thus the H I and [C II] 158 μm data can be brought in agreement if a two-temperature model is assumed for the PDR H I, containing $\sim 70\%$ of the H I mass at about 25 K, and the remaining H I mass at a few hundred degrees or more.

4.2.6. *Clumpy PDRs near Orion B*

The detection of a range of temperatures in the PDRs raises the question of the origin of this temperature structure. A

simple explanation can be found by assuming that the PDR has a layered temperature structure. This approach is justified by theoretical models (e.g., Burton et al. 1990), which show that the warmest gas in the PDR is located close to the H II region, which provides the heating. Alternatively, it may be assumed that the warm and cold gas coexist throughout the PDR, which is most easily realized in an inhomogeneous PDR consisting of cold clumps embedded in a warmer, pervasive interclump medium. There is ample evidence that PDRs are clumpy. Therefore this model is adopted here.

The most compelling evidence for clumpiness in PDRs comes from the large extent of [C II] 158 μm zones, which indicates that the UV radiation penetrates typically several parsecs into the molecular gas surrounding H II regions (Stutzki et al. 1988; Howe et al. 1991). While numerical models of *uniform* PDRs predict UV penetration depths of only 0.01 to 0.1 pc (Tielens & Hollenbach 1985; Sternberg & Dalgarno 1989), this large penetration depth can be explained if the PDRs are clumpy, with clump/interclump density contrasts of about 100 (Stutzki et al. 1988; Howe et al. 1991). The clumps have also been observed directly in optically thin (and thus column density tracing) molecular lines (Stutzki & Güsten 1990). In this model, the volume between the clumps is filled with a warm, low-density gas (Burton et al. 1990).

Within the framework of the cold clump/warm interclump model, the results derived in § 4.2.5 can be understood if the cold H I is located within the dense clumps, where the temperature is low since the attenuation of the radiation field reduces the heating rate, while CO rotational lines provide strong cooling (Burton et al. 1990). The warm H I is located at the clump surfaces where H_2 vibrational heating raises the temperature, and in the interclump gas.

If the interclump density is 1000 cm^{-3}, corresponding to a UV penetration depth of 1 pc in the PDR (Howe et al. 1991), the levels involved in the [C II] 158 μm transitions will not be thermalized. In this case the interclump medium alone cannot produce the observed [C II] emission, which is then produced mainly at the denser clump surfaces. Under the *assumption* of pressure equilibrium of the clump surface with the interclump medium (so that the clumps do not have to be bound by gravitation), the interclump temperature must be higher than that at the clump surface to compensate the density contrast. Thus a plausible model involves an interclump medium with $T \sim 2000$ K and $n \sim 10^3$ cm^{-3}, clump surfaces with $T \sim 200$ K and $n \sim 10^4$ cm^{-3} and clump cores with $T \sim 20$ K and $n \sim 10^5$ cm^{-5}. If the cold material contains $\sim 70\%$ of the mass, as concluded in § 4.2.5, the volume filling factor of the cold clumps will be $\gamma \sim 0.02$.

The choice of parameters above is by no means unique and merely serves to illustrate a possible physical model. For instance, it is possible to have the interclump medium at $T \sim 200$ K and $n \sim 10^4$ cm^{-3}, in which case all of the observed [C II] emission would come from the interclump medium. Pressure equilibrium then again requires the clumps at $T \sim 20$ K to have $n \sim 10^5$ cm^{-3}, but the resulting volume filling factor of the clumps is $\gamma \sim 0.2$. This model is also in agreement with the available data on Orion B, but cannot explain the properties of other PDRs like those near M17 or W3 (Stutzki et al. 1988; Howe et al. 1991). Thus the parameters chosen above are probably more typical of well-studied clumpy PDRs. Models of pressure-confined clumps in molecular clouds have been developed by Bertoldi & McKee (1992) and Verstraete & Sternberg (1993). The latter authors analyze the thermal pressure balance in PDRs to show that a stable, two-phase medium consisting of a hot, low-density interclump medium in pressure equilibrium with cool, dense clumps can exist in PDRs. Although the densities involved are lower than those indicated by the observations, the model is correct in its qualitative features. Furthermore, this model can explain the existence of the small blueshifted cool H I clumps associated with Orion A (van der Werf & Goss 1990b). These clumps, which are not gravitationally bound, and have pressures significantly in excess of standard interstellar pressures, can be confined by a low-density interclump medium that is warm, and thus not detected in the absorption experiment by van der Werf & Goss (1990b).

4.3. *Magnetic Field*

Combining the present magnetic field results with the OH results (Crutcher & Kazès 1983; Kazès & Crutcher 1986; Heiles & Stevens 1986), values for the line-of-sight magnetic field $B_{\|}$ are available for all of the three absorbing layers in front of Orion B: in component A, $B_{\|} = 28$ μG, and in component C, $B_{\|} = 63$ μG. These values can be related to the *total* magnetic field strength $B_{\rm tot} = |\boldsymbol{B}|$ by writing $B_{\rm tot} = xB_{\|}$, where $x \geq 1$. We now simplify the analysis by assuming that x has the same value in all three components, so that the result $B_{\rm tot}^{\rm cmp\ A} < B_{\rm tot}^{\rm cmp\ B} < B_{\rm tot}^{\rm cmp\ C}$ is obtained. As argued in § 4.2.1, component B comes from the dust lane in front of Orion B where $n \sim 10^4$ cm^3, and component C from a compressed (and thus denser, $n \sim 10^5$ cm^{-3}) layer just outside the ionization front. The conclusion that component A is located in the envelope of the background molecular cloud, where its high atomic fraction results from irradiation by the general ISRF implies that typically $n \sim 10^{2-3}$ in this component. At higher densities, the H_2 formation rate would increase strongly and the atomic fraction in this component would be lower than observed (e.g., Federman et al. 1979). Although precise densities in the three absorbing components cannot be derived, it is clear that typical average densities increase in the same sense as $B_{\rm tot}$, in qualitative agreement with simple flux-freezing arguments. The detection of $B_{\|}$ in component C is the first magnetic field detection in a PDR H I layer.

The $B_{\|}$ values can be used to assess the relative importance of the various pressure terms in the three layers. Note that the magnetic field measurements are weighted by the optical depths of the absorbing material, and therefore, since $\tau \propto N(\text{H I, OH})/T$, measure primarily the fields in the cold clumps. Pressure terms have been calculated using $T \sim 20$ K and $\Delta v \sim 2$ km s^{-1} in all three absorbing components, and with the densities listed above. The resulting pressure terms, on the standard interstellar pressure scale where the Boltzmann constant is defined to be unity, are listed in Table 2. Inspection of this table shows that in all three components the thermal pressure is unimportant. In component A magnetic pressure probably dominates. Turbulence likely dominates in component B, and almost certainly in component C, except in the highly unlikely case that $x \gtrsim 10$. As a result, turbulent pressure can create significant structure in components B and C. If magnetic pressure would dominate, clumping would be hindered by the high magnetic tension of the magnetic field frozen in in the density concentrations. The above pressure estimates thus allow significant clumping, in agreement with the clumpy PDR model proposed in § 4.2.6.

Obviously, the uncertainties in the calculated pressure terms are considerable. However, changing the adopted parameters

within the ranges allowed by the data will leave the above qualitative conclusions unaffected. The emerging trend is thus that in the densest (PDR) component the total pressure is highest, and dominated by turbulence. In the intermediate density layer the total pressure is lower and probably still dominated by turbulence. In the less dense molecular cloud envelope the total pressure is lower, and dominated (although perhaps not by far) by magnetic pressure. In even less dense material the total pressure is still lower: Heiles (1989) finds in a number of H I shells (with $n \sim 10$ cm^{-3}) total pressures of typically 5×10^4 cm^{-3} K, totally dominated by magnetic pressure. The commonly accepted standard (thermal) interstellar pressure is still lower: $p_{th} = 4$–8×10^3 cm^{-3} K (Kulkarni & Heiles 1987). The pressure estimates above are in agreement with the conclusion by Chromey et al. (1989) that the cloud envelope forms a pressure link between the cloud interior and the ambient medium.

5. CONCLUSIONS

Analysis of the H I absorption and emission and 21 cm continuum data of the H II region Orion B, and combination of this data with other measurements has led to the following conclusions.

1. There are three kinematically distinct absorbing H I layers in front of Orion B. H I component A at $v_{LSR} \approx 12$ km s^{-1} agrees in velocity with the background molecular cloud, and originates presumably in the envelope of this cloud, extending in front of the H II region. Component B at $v_{LSR} \approx 9.6$ km s^{-1} agrees in velocity with the most prominent molecular absorption lines and originates in the dust lane covering a large fraction of the front side of the H II region. Component C at $v_{LSR} \approx 7$ km s^{-1} agrees in velocity with the ionized gas. Since in addition this component shows structural features of the H II region, this layer is located closest to the H II region, in a region of completely photodissociated gas, swept up by the shock front outside the H II region ionization front. In agreement with this conclusion, this component is largely atomic. This model is essentially identical to the model constructed for the three absorbing H I layers in front of Orion A (Paper I).

2. In addition to H I absorption, H I emission is detected. Strong absorption by foreground H I prohibits detection of the emission except in one of the wings of the emission line, at $v_{LSR} = 15.8$ km s^{-1}, where typical brightness temperatures are about 20 K, with peak values of more than 60 K. It is estimated that the central velocity of the emission is about 12 km s^{-1}, and that brightness temperatures at this velocity are about a factor of 3 higher than at 15.8 km s^{-1}. In view of its velocity, this emission most likely originates in a PDR on the front side of the background molecular cloud. The H I emission peaks in the edge-on PDR near the southern ionization front.

3. PDR H I has been detected in absorption from the front side of the H II region and in emission from behind the H II region. Under the assumption that these foreground and background PDRs have comparable structures, a range of temperatures must exist in the PDRs. The absorption data show that the minimum temperature is less than 20 K, while the emission data imply a maximum temperature of at least 60 K, but most likely at least a factor of 3 higher, according to conclusion 2 above.

4. Due to its low temperature, the absorbing H I contributes a negligible fraction of the observed [C II] 158 μm line emission from the PDRs. The H I emission data and the [C II] measurements can be brought in agreement if the emitting H I has a temperature of at least a few hundred degrees, in agreement with conclusion 3 above.

5. The above conclusions are consistent with a clumpy PDR model, where the cold gas is located in dense clumps and the warmer gas in a lower density interclump medium. If clump-interclump pressure equilibrium is assumed, the density contrast required by the data is about a factor of 10. However, the data are fully consistent with higher density contrasts such as have been invoked for other PDRs. The cold clumps contain probably about 70% of the mass, implying a volume filling factor for the clumps of 0.2 for a density contrast of 10 (0.02 for a density contrast of 100).

6. The line-of-sight component of the magnetic field at 100″ (~ 0.2 pc) resolution is $B_{||} = 28$ μG in component A and 63 μG in component C. Previous OH measurements have yielded $B_{||} = 38$ μG for component B. The relative magnitudes of these values probably reflect a decreasing total magnetic field strength from component C, via component B to component A. The magnetic field strength thus decreases with decreasing density, in qualitative agreement with simple flux-freezing arguments. The total pressure decreases in the same direction, but the importance of magnetic pressure relative to the other pressure terms increases. While in the molecular cloud envelope (component A) the magnetic pressure dominates, it is relatively unimportant in the PDR, where turbulence is the dominant pressure source. The rather extreme clumping that may be present in PDRs may be related to the dominance of turbulent pressure.

The National Radio Astronomy Observatory is operated by Associated Universities, Inc., under a cooperative agreement with the National Science Foundation.

REFERENCES

Allen, R. J., Atherton, P. D., & Tilanus, R. P. J. 1986, Nature, 319, 296
Allen, R. J., Ekers, R. D., & Terlouw, J. P. 1985, in Proc. International Workshop on Data Analysis in Astronomy at Erice, ed. L. Scarci & V. di Gesu (London: Plenum), 271
Anantharamaiah, K. R., Goss, W. M., & Dewdney, P. E. 1990, in IAU Coll. 125, Radio Recombination Lines: 25 Years of Investigations, ed. M. A. Gordon & R. L. Sorochenko (Dordrecht: Kluwer), 123
Anthony-Twarog, B. J. 1982, AJ, 87, 1213
Baars, J. W. M., Genzel, R., Pauliny-Toth, I. I. K., & Witzel, A. 1977, A&A, 61, 99
Bally, J., Langer, W. D., & Liu, W. 1991, ApJ, 351, 176
Barnes, P., & Crutcher, R. 1990, ApJ, 351, 176
Barnes, P., Crutcher, R., Bieging, J., Storey, J., & Willner, S. 1989, ApJ, 342, 883 (BCBSW)
Bertoldi, F., & McKee, C. F. 1992, ApJ, 395, 140
Betz, A. L., Boreiko, R. T., & Zmuidzinas, J. 1990, in Submillimetre Astronomy, ed. G. D. Watt & A. S. Webster (Dordrecht: Kluwer), 117
Bieging, J. H., Wilson, T. L., & Downes, D. 1982, A&AS, 49, 607
Black, J. H., & Van Dishoeck, E. F. 1987, ApJ, 322, 412
Black, J. H., & Willner, S. P. 1984, ApJ, 279, 673
Burton, M. G., Hollenbach, D. J., & Tielens, A. G. G. M. 1990, ApJ, 365, 620
Cameron, A. G. W. 1973, Space Sci. Rev., 15, 121
Chromey, F. R., Elmegreen, B. G., & Elmegreen, D. M. 1989, AJ, 98, 2203
Crawford, M.J., Genzel, R., Townes, C. H., & Watson, D. M. 1985, ApJ, 291, 755
Crawford, M. K., Lugten, J. B., Fitelson, W., Genzel, R., & Melnick, G. 1986, ApJ, 303, L57
Crutcher, R. M., Henkel, C., Wilson, T. L., Johnston, K. J., & Bieging, J. H. 1986, ApJ, 307, 302
Crutcher, R. M., & Kazès, I. 1983, A&A, 125, L23

Dewdney, P. E., & Roger, R. S. 1982, ApJ, 255, 264
———. 1986, ApJ, 307, 275
Elmegreen, B. G. 1989, ApJ, 338, 178
Evans, N. J., Mundy, L. G., Davis, J. H., & Vanden Bout, P. A. 1987, ApJ, 312, 344
Federman, S. R., Glassgold, A. E., & Kwan, J. 1979, ApJ, 227, 466
Flower, D. R. 1988, J. Phys. B., 21, L451
Flower, D. R., & Launay, J.-M. 1977, J. Phys. B, 10, 3673
Gatley, I., Hasegawa, T., Suzuki, H., Garden, R., Brand, P., Lightfoot, J., Glencross, W., Okuda, H., & Nagata, T. 1987, ApJ, 318, L73
Gaume, R. A., Johnston, K. J., & Wilson, T. L. 1992, ApJ, 388, 489
Genzel, R., Harris, A. I., & Stutzki, J. 1989, in Infrared Spectroscopy in Astronomy, ed. B. H. Kaldeich (ESA SP-290), 115
Gillett, F. C., & Houck, J. R. 1991, Phys. Today, 44-4, 32
Gordon, M. A. 1969, ApJ, 158, 479
Goss, W. M., Winnberg, A., Johansson, L. E. B., & Fournier, A. 1976, A&A, 46, 1
Goudis, C. 1982, The Orion Complex: a Case Study of Interstellar Matter (Dordrecht: Reidel)
Graf, U. U., Genzel, R., Harris, A. I., Hills, R. E., Russell, A. P. G., & Stutzki, J. 1990, ApJ, 358, L49
Graf, U. U., Eckart, A., Genzel, R., Harris, A. I., Poglitsch, A., Russell, A. P. G., & Stutzki, J. 1993, ApJ, in press
Grasdalen, G. L. 1974, ApJ, 193, 373
Green, D. A. 1991, MNRAS, 253, 350
Hartquist, T. W., & Sternberg, A. 1991, MNRAS, 248, 48
Hayashi, M., Hasegawa, T., Gatley, I., Garden, R., & Kaifu, N. 1985, MNRAS, 215, 31P
Heiles, C. 1989, ApJ, 336, 808
Heiles, C., & Stevens, M. 1986, ApJ, 301, 331
Howe, J. E., Jaffe, D. T., Genzel, R., & Stacey, G. J. 1991, ApJ, 373, 158
Hubble, E. P. 1922, ApJ, 56, 162
Jaffe, D. T., et al. 1993, in preparation
Kazès, I., & Crutcher, R. M. 1986, A&A, 164, 328
Krügel, E., Thum, C., Martin-Pintado, J., & Pankonin, V. 1982, A&AS, 48, 345
Kulkarni, S. R., & Heiles, C. 1987, in Interstellar Processes, ed. D. J. Hollenbach & H. A. Thronson (Dordrecht: Reidel), 87
Kurtz, N. T., Smyers, S. D., Russell, R. W., Harwit, M., & Melnick, G. 1983, ApJ, 264, 538
Lada, E. A., DePoy, D. L., Evans, N. J., & Gatley, I. 1991a, ApJ, 368, 432
Lane, A. P., Haas, M. R., Hollenbach, D. J., & Erickson, E. F. 1990, ApJ, 361, 132
Lasker, B. M. 1966, ApJ, 143, 700
Launay, J.-M., & Roueff, E. 1977, J. Phys. B, 10, 879
Löbert, W., & Goss, W. M. 1978, MNRAS, 183, 119
Lockhart, I. A., & Goss, W. M. 1978, A&A, 67, 355 (LG)
Maddalena, R. J., Morris, M., Moscowitz, J., & Thaddeus, P. 1986, ApJ, 303, 375
Mundy, L. G., Evans, N. J., Snell, R. L., & Goldsmith, P. F. 1987, ApJ, 318, 392
Panagia, N. 1973, AJ, 78, 929
Pankonin, V., Walmsley, C. M., Wilson, T. L., & Thomasson, P. 1977, A&A, 57, 341
Pauliny-Toth, I. I. K., Wade, C. M., & Heeschen, D. S. 1966, ApJS, 13, 65
Read, P. L. 1981, MNRAS, 194, 863
Richer, J. S., Hills, R. E., Padman, R., & Russell, A. P. G. 1989, MNRAS, 241, 231
Roger, R. S., & Dewdney, P. E. 1992, ApJ, 256, 127
Roger, R. S., & Irwin, J. A. 1982, ApJ, 256, 127
Russell, A. P. G., Hills, R. E., & Padman, R. 1987, MNRAS, 226, 237
Russell, R. W., Melnick, G., Gull, G. E., & Harwit, M. 1980, ApJ, 240, L99
Russell, R. W., Melnick, G., Smyers, S. D., Kurtz, N. T., Gosnell, T. R., Harwit, M., & Werner, M. W. 1981, ApJ, 250, L35
Sanders, D. B., & Willner, S. P. 1985, ApJ, 293, L39
Schenewerk, M. S., Snyder, L. E., Hollis, J. M., Jewell, P. R., & Ziurys, L. M. 1988, ApJ, 328, 785
Snell, R. L., Mundy, L. G., Goldsmith, P. F., Evans, N. J., & Erickson, N. R. 1984, ApJ, 276, 625
Spitzer, L. 1978, Physical Processes in the Interstellar Medium (New York: Wiley)
Stacey, G. J., Geis, N., Genzel, R., Lugten, J. B., Poglitsch, A., Sternberg, A., & Townes, C. H. 1991, ApJ, 373, 423
Stark, A. A., & Bally, J. 1982, in Regions of Recent Star Formation, ed. R. S. Roger & P. E. Dewdney (Dordrecht: Reidel), 329
Sternberg, A. 1988, ApJ, 332, 400
Sternberg, A., & Dalgarno, A. 1989, ApJ, 338, 197
Stutzki, J., & Güsten, R. 1990, ApJ, 356, 513
Stutzki, J., Stacey, G. J., Genzel, R., Harris, A. I., Jaffe, D. T., & Lugten, J. B. 1988, ApJ, 332, 379
Subrahmanyan, R. 1991, MNRAS, 254, 719
Terzian, V., Mezger, P. G., & Schraml, J. 1968, Astrophys. Letters, 1, 153
Thompson, A. R., Clark, B. G., Wade, C. M., & Napier, P. J. 1980, ApJS, 44, 51
Thompson, R. I., Thronson, H. A., & Campbell, B. G. 1981, ApJ, 249, 622
Thronson, H. A., Lada, C. J., Schwartz, P. R., Smith, H. A., Smith, J., Glaccum, W., Harper, D. A., & Loewenstein, R. F. 1984, ApJ, 280, 154
Tielens, A. G. G. M., & Hollenbach, D. J. 1985, ApJ, 291, 722
Tilanus, R. P. J., & Allen, R. J. 1989, ApJ, 339, L57
Troland, T. H., Heiles, C., & Goss, W. M. 1989, ApJ, 337, 342
van der Werf, P. P., Dewdney, P. E., Goss, W. M., & Vanden Bout, P. A. 1989, A&A, 216, 215
van der Werf, P. P., & Goss, W. M. 1989, A&A, 224, 209 (Paper I)
———. 1990a, A&A, 238, 296 (Paper II)
———. 1990b, ApJ, 364, 157
van der Werf, P. P., Goss, W. M., & Vanden Bout, P. A. 1988, A&A, 201, 311
Verstraete, L., & Sternberg, A. 1993, in preparation
Wakker, B. P., & Schwarz, U. J. 1988, A&A, 200, 312
Watson, D. M. 1984, in Galactic and Extragalactic Infrared Spectroscopy, ed. M. F. Kessler & J. P. Phillips (Dordrecht: Reidel), 193